The Astrophysical Journal Supplement Series, 201:28 (11pp), 2012 August doi:10.1088/0067-0049/201/2/28

MEASUREMENT OF THE Fe VIII–Fe XVI 3–3 EMISSION IN THE EXTREME ULTRAVIOLET AND COMPARISON WITH CHIANTI

P. Beiersdorfer[1,2] and J. K. Lepson[1]
[1] Space Sciences Laboratory, University of California, Berkeley, CA 96720, USA
[2] Lawrence Livermore National Laboratory, Physics Division, Livermore, CA 94550, USA
Received 2012 February 13; accepted 2012 June 17; published 2012 July 25

ABSTRACT

Laboratory measurements of the $n = 3$ to $n = 3$ emission from M-shell iron ions are presented and compared to synthetic spectra from the CHIANTI spectral model. The measurements cover the range 170–290 Å and are made at an electron density of about 10^{11} cm^{-3}. Emission from Fe VIII through Fe XVI has been identified. Excellent agreement with CHIANTI predictions is found for most lines. Twenty weaker features are noted in the laboratory data that are either absent in CHIANTI or have recently been added and correspond to lines that have not been verified by experimental measurements. A few of these lines may have already been observed (but not yet identified) in the Sun. The features are attributed to emission from various charge states of iron, notably Fe IX and Fe XIII, and two features have been identified as transitions in Fe VIII, i.e., the $3p^6 3d\ ^2D_{5/2}$–$3p^5 3d^2\ ^2P_{3/2}$ and the $3p^6 3d\ ^2D_{3/2}$–$3p^5 3d^2\ ^2P_{1/2}$ transitions at 225.25 ± 0.12 and 226.35 ± 0.10 Å, respectively. Seven lines in Fe XI, Fe XII, and Fe XIII between 200 and 205 Å are noted for which the wavelengths in the CHIANTI database disagree with those in the current database of the National Institute of Standards and Technology. Our measurements of five of these lines appear to agree with the assignments used in CHIANTI.

Key words: atomic data – atomic processes – line: formation – line: identification – stars: coronae – Sun: X-rays, gamma rays – X-rays: general

Online-only material: color figures

1. INTRODUCTION

The 3–3 emission from M-shell iron ions above 170 Å is diagnostically very important, as it provides information on the density and temperature of the emitting medium. It has been observed in the past in various stellar coronae by the *Extreme-Ultraviolet Explorer* (Schrijver et al. 1995; Schmitt et al. 1996a, 1996b) and with very high resolution in the Sun by various flights of the *Solar EUV Rocket Telescope and Spectrograph* (*SERTS*) (Thomas & Neupert 1994) as well as by the RES-C spectrograph on the *CORONAS-I* mission (Zhitnik et al. 1999). The solar emission above 170 Å was also observed with moderate resolution by the Cosmic Hot Interstellar Plasma Spectrometer (Lepson et al. 2008; Sirk et al. 2010). Currently, stellar emission below about 185 Å can be observed with the LETGS instrument on *Chandra*, while the solar emission is being observed with the EUV Imaging Spectrometer (EIS) on *Hinode*, which focuses on the region 170–210 Å and 250–290 Å (Young et al. 2007). The Extreme Ultraviolet Variability Experiment on the *Solar Dynamics Observatory* (*SDO*) spacecraft also observes this spectral band but with greatly reduced resolution (Woods et al. 2011). Moreover, three of the six iron line channels of the Atmospheric Imaging Assembly (AIA) aboard *SDO* are centered on lines in this region, i.e., the Fe IX line at 171 Å, a mixture of Fe XII and Fe XXIV lines at 194 Å, and the Fe XIV line at 211 Å (Lemen et al. 2012).

The interpretation of spectral data relies on accurate and complete plasma emission models. One of the most widely used spectral models is CHIANTI (Landi et al. 2006, 2012; Dere et al. 2009). Earlier laboratory measurements of iron spectra have found some deficiencies in the CHIANTI line list, e.g., the measurements of Fe VIII through Fe X (Beiersdorfer et al. 1999b; Lepson et al. 2002). However, these measurements have been at shorter wavelengths, i.e., at wavelengths well below 170 Å. A test of the CHIANTI model in the wavelength range above 170 Å has recently been made for Fe XIII by Yamamoto et al. (2008). A comparison of spectral data from the Large Helical Device and the Livermore EBIT-II electron beam ion trap with synthetic spectra from CHIANTI revealed very good agreement. The new spectral measurements afforded by the *Hinode* EIS instrument, however, have led to new line identifications coupled with new theoretical calculations (Ishikawa & Vilkas 2008; Young 2009; Young & Landi 2009; Del Zanna 2009, 2010, 2011; Del Zanna et al. 2010; Liang et al. 2010; O'Dwyer et al. 2012). Many of these new data have been included in the newest version of CHIANTI, i.e., version 7.0, which has been released recently (Landi et al. 2012). As a result, revisions in CHIANTI since version 5.1 include data for Fe VIII, Fe IX, and Fe XI among others.

In the following, we extend our earlier comparison between laboratory spectra and CHIANTI modeling result (Yamamoto et al. 2008) to the emission from charge states between Fe VIII and Fe XVI. The measurements cover the wavelength range 170–290 Å and are made at an electron density of about 2×10^{11} cm^{-3}. We find excellent agreement between CHIANTI and the laboratory measurement in the 170–290 Å range. We have also identified several weak features that are not reproduced by CHIANTI. Others correspond to lines added in the recent revision or to theoretical lines that have not yet been verified experimentally. While the total flux in these features is rather small—the strongest of these features have a few per cent of the intensity of the strongest lines from the same charge state in this wavelength band, some of the missing lines may have already been observed (and not identified) in *SERTS* or EIS observations.

Our aforementioned investigation (Yamamoto et al. 2008) had uncovered some discrepancies in the 200–205 Å region between

the line list employed by CHIANTI and the iron transitions listed in the spectral data base of the National Institute of Standards and Technology (NIST 2012). We find seven lines in Fe XI, Fe XII, and Fe XIII in this interval for which the wavelengths in the CHIANTI database disagree with those in the current database given by NIST. We have attempted to clarify this discrepancy by determining the originating charge state and wavelength of each line in question. The results for the five lines we were able to study favor the atomic data used in CHIANTI.

2. MEASUREMENTS

The spectral data were recorded at the EBIT-II electron beam ion trap at the Lawrence Livermore National Laboratory (Beiersdorfer 2008). This machine has been used for a variety of laboratory astrophysics measurements in the past, as summarized by Beiersdorfer (2003). It typically operates at densities below 10^{12} cm^{-3} (Chen et al. 2004). Using the current scaling of the electron density from the measurements of Chen et al. (2004), we estimate the density during the present measurements to be around 2×10^{11} cm^{-3}. This represents the "high"-density limit for the iron lines in the wavelength region of interest, i.e., predictions show that the emission of these lines is no longer sensitive to the electron density at such high densities. By contrast, the line intensities are predicted to change significantly in the range around 10^{9}–10^{10} cm^{-3} (cf. predictions by, for example, Liang et al. 2009), which is why they are very good spectral diagnostics of electron density in the Sun and stellar atmospheres.

The present measurements follow the procedures employed in our earlier study of Fe XIII (Yamamoto et al. 2008) and in other measurements of iron lines (Savin et al. 1996; Gu et al. 1999; Drake et al. 1999; Beiersdorfer et al. 1999b; Lepson et al. 2000; Brown et al. 2001; Chen et al. 2002). In the present experiments, iron was injected into the trap in the form of iron pentacarbonyl via a gas injector. The electron beam energy ranged from 190 to 513 eV, i.e., from above the ionization energy of 150 eV needed to produce Fe^{8+} ions to an energy sufficient to produce Fe^{16+} ions. The beam energies at which spectra were taken were chosen so that roughly at each new energy one new iron charge state was produced and added lines to the observed spectrum. The emission from lower charge states continued to be observed because of the fact that neutral iron was continuously injected into the trap. Moreover, the measurements were integrated in time over the ionization phase.

A series of spectra taken at different beam energies is shown in Figure 1. In particular, the figure shows spectra obtained at electron beam energies of 190 eV, 263 eV, and 313 eV. At the lowest energy, only iron ions with charge $q \leqslant 9+$ are produced. The dominant lines seen are thus from Fe IX and Fe X, i.e., for example, the strong Fe IX line at 171 Å. At the next higher energy, Fe^{10+} ions can be produced as well, and strong emission from the well known Fe XI lines is seen. Finally, at the highest of the three energies, lines from Fe XII become prominent as well, including the cluster of Fe XII lines around 194 Å, which, similar to the Fe IX line at 171 Å, is of interest to one of the iron channels of the AIA.

The spectra were recorded with a grazing-incidence spectrometer (Beiersdorfer et al. 1999a). This instrument employs an average 1200 line mm^{-1} flat-field grating with a 3° angle of incidence. Spectra were recorded with a back-illuminated, liquid nitrogen-cooled charge-coupled device (CCD) camera. It consists of a one inch square array of 1024 × 1024 pixels. The instrumental resolution is about 0.3 Å which gives a resolving power of ~600 at 200 Å. The camera continuously integrates the spectral emission from the trap. No shutter is used.

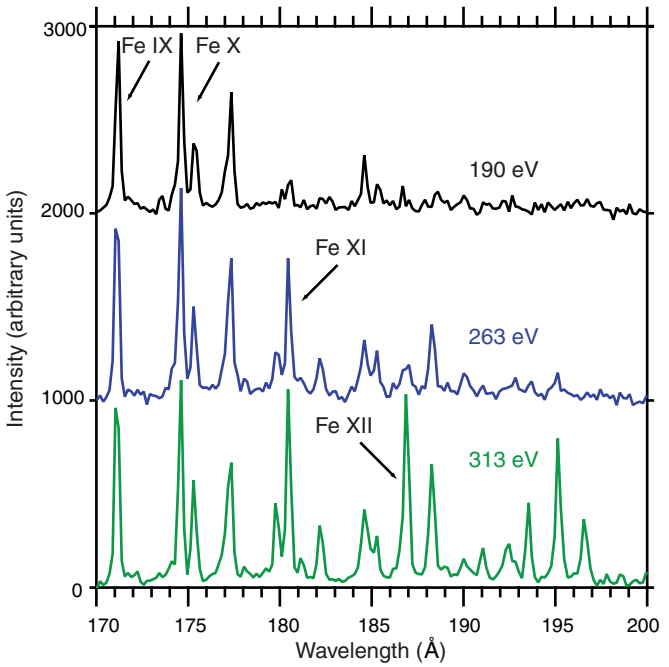

Figure 1. Iron spectra recorded on the EBIT-II electron beam ion trap at Livermore with different electron beam energies. The iron charge states produced at the different energies are indicated.

(A color version of this figure is available in the online journal.)

A foil comprised of a 2000 Å thick aluminum layer on top of 1000 Å of paralene was placed in front of the grating in order to screen out emission from lines with wavelengths below 170 Å. This was necessary to avoid spectral contamination from higher-energy iron lines that would show up in second-, third-, or fourth-order reflection (Beiersdorfer et al. 1999a). Although the $n = 3$–3 emission of interest here is typically much stronger than the emission from the $n = 4$ (or higher) level to the $n = 3$ level, blending from higher orders can otherwise be significant especially when studying weak 3–3 lines.

The trap was periodically emptied and filled (on the order of seconds). This prevented the build-up of heavy impurity ions in the trap. Indeed, no evidence of lines from heavy impurities was found in our measurements, even when taking spectra in the absence of iron injection. The total integration time to collect a single spectrum was 30 minutes. To increase the signal-to-noise ratio, multiple 30 minute spectra were added.

The wavelength scale was established using the well known K-shell emission lines of nitrogen, in particular the N VII Lyα line and the N VI resonance line commonly referred to as w, as described by Beiersdorfer et al. (1999a). These spectra were observed in higher (seventh, eighth, ninth) orders upon injection of nitrogen gas into EBIT-II. The energies of these lines are high enough to pass through the aluminum filter without appreciable attenuation. The wavelengths of the strong iron emission lines in this wavelength region are well known, and we have not attempted to improve upon those data.

Spectra were also taken without an active trap, i.e., without a potential applied to the trap electrodes. These spectra enabled us to determine the level of background emission (including visible light from the electron-gun filament, to which the CCD camera is sensitive). The background emission was then subtracted from

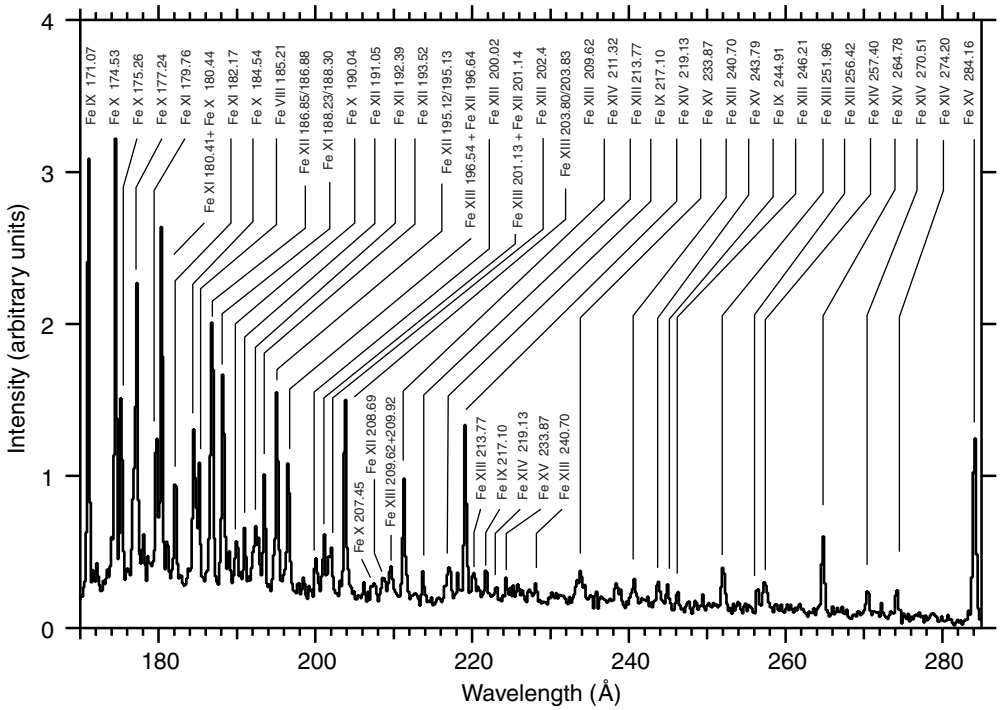

Figure 2. Overview of the spectral data recorded on the EBIT-II device showing emission from Fe VIII through Fe XV. Features are labeled by the spectrum number and wavelength, as given by CHIANTI (Dere et al. 1997; Landi et al. 2006). The spectrum represents a summation of spectra taken at different excitation energies.

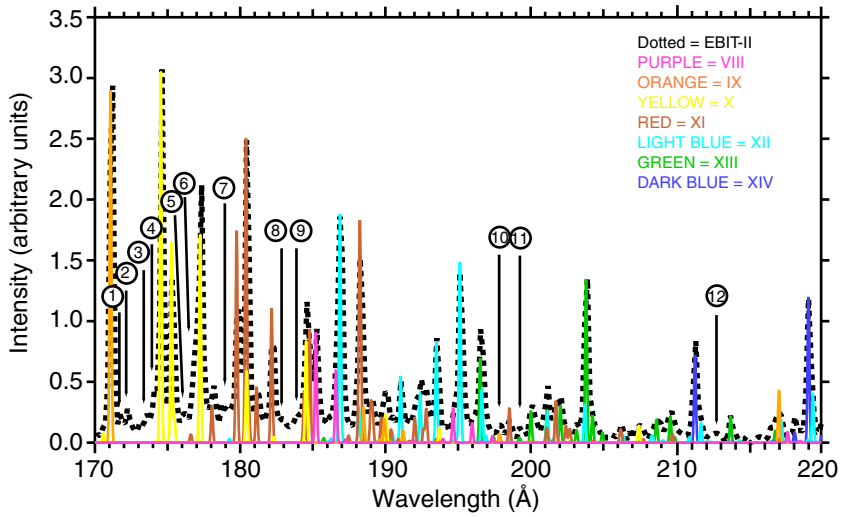

Figure 3. Detailed iron emission between 170 and 220 Å. The spectrum was recorded on the EBIT-II electron beam ion trap at Livermore (dashed, black trace). Also shown is the predicted emission from CHIANTI for Fe VII (purple trace), Fe IX (orange trace), Fe X (yellow trace), Fe XI (red trace), Fe XII (light blue trace), Fe XIII (green trace), and Fe XIV (dark blue trace). The predicted intensities are adjusted for each charge state to that of the strongest line observed in the measurement. Features that are not reproduced by the CHIANTI V7.0 model are labeled 1 through 9 and 12. Features 10 and 11 are newly included in V7.0.

(A color version of this figure is available in the online journal.)

the iron to yield background-corrected spectra (Lepson et al. 2002).

3. RESULTS

An overview of the line emission observed between 170 and 290 Å is shown in Figure 2. The spectrum represents the sum of spectra recorded at electron beam energies between 363 and 513 eV, which means that lines from all charge states produced during the experiment are seen. In particular, the spectrum shows the prominent lines from Fe IX at 171 Å, Fe X at 174.5 Å, Fe XI at 180.4 Å, Fe XII at 186.9 and 195.1 Å, Fe XIII at 203.8 Å, Fe XIV at 219.1 Å, and Fe XV at 284.2 Å. Although Fe^{15+} ions were produced during the experiments, the region from 170 to 290 Å has no Fe XVI lines except for a very weak feature at 251.1 Å.

A close-up of the spectral emission between 170 and 220 Å is shown in Figure 3. This wavelength region contains lines from Fe VIII through Fe XIV. Also shown are the predictions from the CHIANTI V7.0 spectral model (Landi et al. 2012). Because the electron density of the EBIT-II device is sufficiently high so that the emission can be considered to be in the high-density limit, i.e., the emission does not depend on the exact value of the density, we have compared the data with CHIANTI spectra calculated at a density of 10^{15} cm^{-3}. For comparison, we have treated the ionization balance in our measurements as a free parameter. As a consequence, we have normalized the intensity

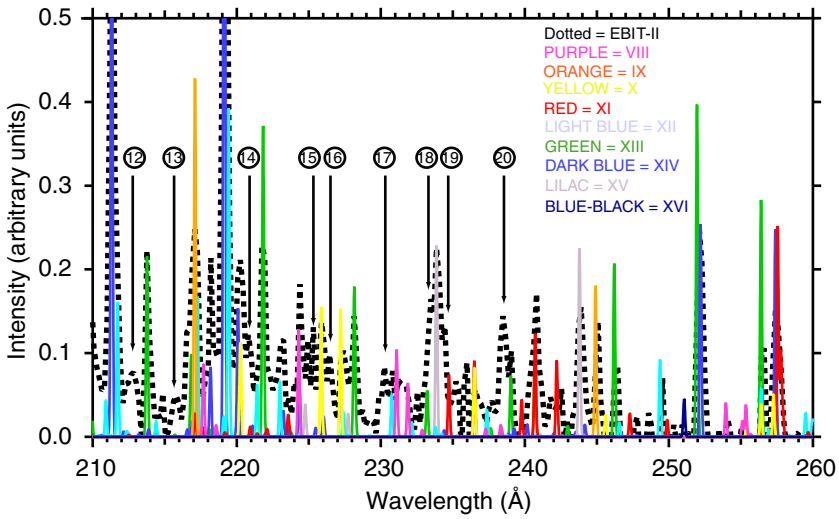

Figure 4. Detailed iron emission between 210 and 260 Å. The spectrum was recorded on the EBIT-II electron beam ion trap at Livermore (dashed, black trace). Also shown is the predicted emission from CHIANTI for Fe VII (purple trace), Fe IX (orange trace), Fe X (yellow trace), Fe XI (red trace), Fe XII (light blue trace), Fe XIII (green trace), Fe XIV (dark blue trace), Fe XIV (dark blue trace), Fe XV (lilac trace), and Fe XVI (blue trace). The predicted intensities are adjusted for each charge state to that of the strongest line observed in the measurement. Features that are not reproduced by the CHIANTI model are labeled 12 through 20.

(A color version of this figure is available in the online journal.)

of the strongest line of each charge state predicted by CHIANTI to the strongest line in the measured spectrum. CHIANTI also includes predictions for many iron lines, in particular Fe IX lines, that have not been verified by experiment or observation. The calculated wavelengths of these lines may be uncertain by several Å. As a result, we have not included such lines in the CHIANTI spectra. However, these calculated lines will be discussed in more detail below.

There is excellent agreement between the CHIANTI model and the EBIT-II data. This agreement extends not only to the wavelength but also to the intensity of a given line. As can be seen from Figure 3 the CHIANTI model reproduces the vast majority and all of the strongest spectral features. It is interesting to note that changes in the line intensities that occurred between CHIANTI V5.1, V6.0, and V7.0 do not substantially affect the quality of the agreement with our ("high" electron density) measurements.

There are only a few weak features in the spectrum in Figure 3 that are not reproduced by the CHIANTI V7.0 model. These features are labeled 1 through 9 and 12 in Figure 3. Features 10 and 11 correspond to lines missing in early versions of CHIANTI. Although these features are weak, they are experimentally reproducible and thus significant. Moreover, they are as strong or stronger than features that are included in the CHIANTI model.

The CHIANTI model also makes no predictions for lines in the region between the strongest Fe IX at 171 Å and the strongest Fe X line just below 175 Å. The experimental spectrum clearly shows emission in this 3.5 Å interval. We have distinguished four features, labeled 1 through 4, to describe the emission in this interval. Similarly, we find excess flux on the shoulders of or between other strong lines at somewhat longer wavelengths. These we have labeled features 5 through 9.

A close-up of the spectral emission between 210 and 260 Å is shown in Figure 4. This wavelength region contains lines from Fe VIII through Fe XVI, although only Fe XII, Fe XIII, and Fe XIV contribute to the strongest observed lines. Note that the intensity scale is increased by a factor of six from that used in Figure 3. This means that many of the lines are weaker than those in Figure 3.

Also shown in Figure 4 are the predictions from the CHIANTI V7.0 spectral model (Landi et al. 2012). Again, there is excellent agreement between the CHIANTI model and the EBIT-II data. We, however, note that among the stronger lines, there is some disagreement. The intensity of the Fe IX line near 217 Å appears to be overpredicted by almost a factor of two, and the Fe XIII lines at 222, 246, 252, and 257 Å are overpredicted by factors between 1.5 and 3. The latter disagreement was already found when comparing to CHIANTI V5.1, but it became larger in V7.0.

As is the case in the 170–210 Å region, some weaker features in this wavelength region are not predicted by the CHIANTI V7.0 high-density model. These are labeled 12 through 20. The strongest solitary feature in this spectrum not described by the CHIANTI model is feature 20. The other features are in between strong lines or on the shoulders of other lines.

Several of the unknown lines in Figure 4 can be enhanced by suppressing lines from Fe XV. This is illustrated in Figure 5 where we have summed spectra produced at electron beam energies in the range of 263–363 eV, i.e., at beam energies too low to produce lines from Fe XV. In this case, features 18 and 19 are much more prominent. Feature 15, 16, and 17 are more prominent as well, although they border on lines from lower charge states than Fe XV. This is probably mainly a statistical artifact.

The spectrum from 210 to 260 Å may contain additional unidentified peaks at wavelengths longer than 240 Å. However, the signal to noise is too small to make reliable determinations, and we have refrained from pointing out such additional unidentified features.

A summary of the 18 experimental features not reproduced by the CHIANTI V7.0 model is given in Table 1. We have also included the two features that can be explained by the recent additions to V7.0. Here, we list the approximate wavelength of each feature together with a possible range of charge states that are likely to produce the feature. These ranges are based on when these features appeared in the measured spectra as the electron beam energy was changed. Because these features are generally weak, such a determination is inherently inexact. For example, feature 1 at 171.73 ± 0.05 Å has been already noted

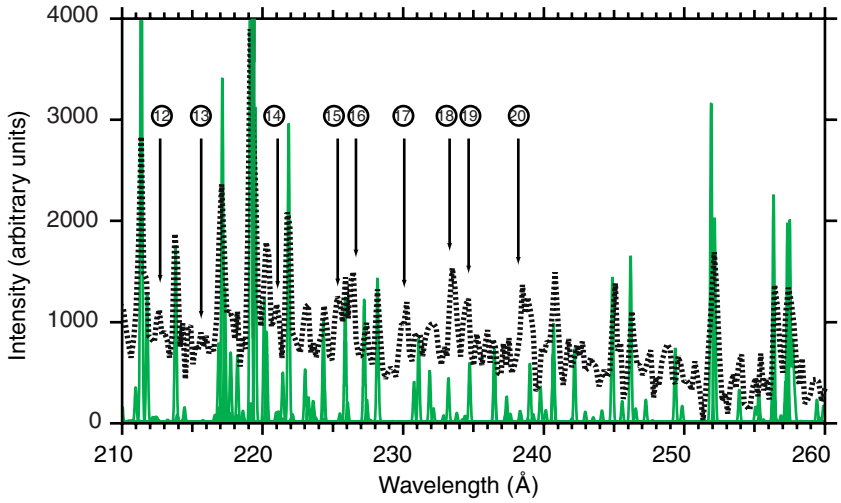

Figure 5. Detailed iron emission between 210 and 260 Å. The spectrum (dashed, black trace) was recorded on the EBIT-II electron beam ion trap at Livermore at electron beam energies below those to produce lines from Fe XV. The predicted emission from CHIANTI for Fe VIII through Fe XIV is shown as a green trace (cf. Figure 4). Features that are not reproduced by the CHIANTI model are labeled 12 through 20.

(A color version of this figure is available in the online journal.)

Table 1
Wavelengths and Associated Ionization Stage of Spectral Features Not Predicted by CHIANTI

Feature	Wavelength (Å)	Parent Ion	Comment
1	171.73 ± 0.05	⩽Fe X	...
2	172.24 ± 0.05	⩽Fe XI	Possibly matches unidentified SERTS-95 line at 172.335 Å
3	173.55 ± 0.05	⩽Fe IX	Prominent at the lowest electron energies only
4	174.11 ± 0.07	⩽Fe X	May be in part formed by $3s^2 3p^5 3d\ ^3D_1$–$3s^2 3p^4 3d^2\ ^3D_1$ transition in Fe IX
5	176.15 ± 0.10	⩽Fe X	...
6	176.80 ± 0.10	⩽Fe X	Coincides with $3s^2 3p^5 3d\ ^3F_4$–$3s^2 3p^4 3d^2\ ^3D_3$ Fe IX transition identified by Young & Landi (2009)
7	178.80 ± 0.10	⩽Fe X	...
8a	182.70 ± 0.05	⩽Fe X	...
8b	182.95 ± 0.08	⩽Fe XII	Possibly matches unidentified line in *Hinode*
9	183.90 ± 0.08	⩽Fe X	Seen at the lowest electron energies only; SERTS-95 shows two weak, unlabeled lines at ∼183.85 and 184.03 Å
10	197.98 ± 0.09	⩽Fe XII	Matches $3s^2 3p^5 3d\ ^1P_1$–$3s^2 3p^5 4p\ ^1S_0$ Fe IX line identified by Young (2009)
11	199.40 ± 0.15	⩾Fe XIII	Matches$3s 3p^3\ ^3D_3$–$3s^3 p^2 3d\ ^3F_4$ Fe XIII line in CHIANTI V7.0
12	212.60 ± 0.10	≈Fe XI	...
13	215.90 ± 0.10	⩾Fe XIII	Seen in spectra below 360 eV beam energy
14	220.90 ± 0.10	⩽Fe XI	Tentatively identified as $3s^2 3p^4\ ^3P_2$–$3s^2 3p^3 3d\ ^3G_3$ transition in Fe XI
15	225.25 ± 0.12	⩽Fe X	Identified as $3p^6 3d\ ^2D_{5/2}$–$3p^5 3d^2\ ^2P_{3/2}$ transition in Fe VIII
16	226.35 ± 0.10	⩽Fe X	Identified as $3p^6 3d\ ^2D_{3/2}$–$3p^5 3d^2\ ^2P_{1/2}$ transition in Fe VIII
17	230.06 ± 0.08	≈Fe XIII	...
18	233.50 ± 0.10	≈Fe XIII	Close to Fe XIII line at 233.24 Å and possibly is the same line; model underpredicts intensity
19	234.60 ± 0.10	≈Fe XIII	...
20a	238.50 ± 0.08	≈Fe XIII	...
20b	238.20 ± 0.10	⩽Fe X	Matches wavelength of $3p^6 3d\ ^2D_{5/2}$–$3p^6 4s\ ^2S_{1/2}$ transition in Fe VIII; model underpredicts intensity

in spectra produced at low electron beam energies when lines of Fe X were first visible. While this implies that the line might emanate from Fe X, it is nevertheless possible that it emanates from an even lower charge state but was not seen in those spectra because of a poor signal-to-noise ratio. As a result, we only give an upper bound of the parent charge state. The same is true for features 2 through 9 and 14 through 16. In the case of features 11 and 13 the experimental data allow us to give only a lower bound on the parent charge state. By contrast, the data strongly indicate that features 17 through 20 are from Fe XIII, and feature 12 is likely from Fe XI.

We note that it is possible that a given unidentified feature is a blend of several lines, which may or may not emanate from a single charge state. This appears to be the case for feature 20.

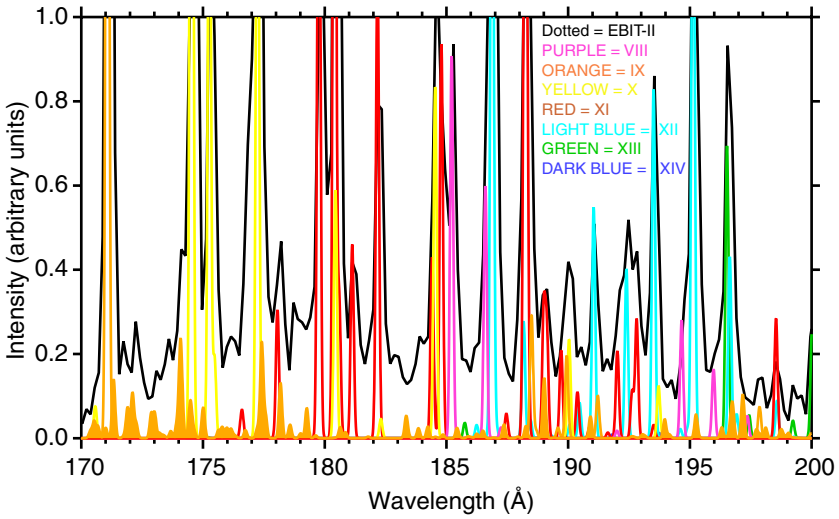

Figure 6. Iron emission between 170 and 220 Å showing the unverified predictions from Fe IX included in CHIANTI V7.0 together (solid trace) with the measured spectrum and the predicted emission from verified lines. The color coding is the same as in Figure 1.

(A color version of this figure is available in the online journal.)

Here, an Fe XIII line seems blended with a line from a lower ionization state, such as Fe X or below.

4. COMPARISON TO CHIANTI V7.0, *HINODE*, AND *SERTS* DATA

In the following, we discuss each of the 20 features presented in Table 1 by comparison with unverified theoretical data in the CHIANTI V7.0 line list (Landi et al. 2012), if available. We also compare to spectral information in this region from *SERTS* observations (Brosius et al. 1998) and from recent analyses of *Hinode* EIS spectra (Young & Landi 2009; Del Zanna 2012).

4.1. Feature 1

CHIANTI V7.0 lists an Fe XX line at 171.725 Å, which closely matches the 171.73 ± 0.05 wavelength of feature 1. However, this line cannot be excited by the beam energies in our measurements and, thus, can be ruled out.

CHIANTI V7.0 also lists a set of theoretical Fe IX lines with unverified wavelengths. We have plotted these predictions in Figure 6, as they give guidance on the relative intensity of the known lines compared to the unverified lines. One of these unverified lines, due to the $3s^2 3p^5 3d\ ^3P_2$–$3s^2 3p^4 3d^2\ ^3P_1$ transition, is reasonably close by at 171.898 Å. Together with the $3s^2 3p^5 3d\ ^3P_2$–$3s^2 3p^4 3d^2\ ^3P_2$ transition listed at 172.103 Å, this line might form feature 1. However, given the uncertainty in the theoretical wavelengths and the number of weak, unverified Fe IX lines it is not possible to make an identification.

4.2. Feature 2

Feature 2 at 172.24 ± 0.05 Å is more intense than feature 1. Its wavelength matches very well that of another Fe IX line in the CHIANTI V7.0 unverified line list at 172.260 Å. But the theoretical intensity is too small. Moreover, feature 2 appears to be produced at a slightly higher threshold energy, which indicates that it may be an Fe X or Fe XI line.

The *SERTS* spectrum reported by Brosius et al. (1998) shows an unidentified line at 172.335 Å, which matches the wavelength of feature 2. It is, thus, possible the line observed with *SERTS* is identical to feature 2, and, therefore, is an Fe X or Fe XI line.

4.3. Feature 3

Feature 3 at 173.55 ± 0.05 Å is prominent only at the lowest excitation energies, which indicates it comes from Fe IX or lower. CHIANTI has no close-by Fe IX line with sufficient intensity to account for this feature. However, it is possible that the two theoretical Fe IX lines listed at 172.870 and 173.018 Å in CHIANTI need to be shifted to longer wavelength, or that some of the many unverified theoretical Fe IX lines listed above 174 Å need to be shifted to shorter wavelength, and thus form this feature. However, as is the case with features 1 and 2, the theoretical data in CHIANTI are too uncertain to identify this feature.

4.4. Feature 4

This feature sits on the shoulder of the strong Fe X line at 174.53 Å. The wavelength of the feature (174.11 ± 0.07 Å) matches very well the theoretical wavelengths of three Fe IX lines listed in CHIANTI V7.0. These three lines blend to form the strongest Fe IX feature below 175 Å, as seen in Figure 6. The strongest of the three lines is the $3s^2 3p^5 3d\ ^3D_1$–$3s^2 3p^4 3d^2\ ^3D_1$ transition at 174.142 Å. The intensity of these unverified lines and the experimental data also match well. This, plus the experimental determination that the feature likely stems from Fe IX, leads us to suggest that feature 4 is produced, at least in part, by the $3s^2 3p^5 3d\ ^3D_1$–$3s^2 3p^4 3d^2\ ^3D_1$ transition.

4.5. Feature 5

Feature 5 has a wavelength of 176.15 ± 0.10 Å. This wavelength is very close to the theoretical wavelength of an Fe IX line in CHIANTI V7.0. The predicted intensity appears, however, too weak to account for this feature (cf. Figure 6).

A better candidate based on intensity is the predicted Fe IX line at 177.418, as seen from Figure 6. In fact, this unverified line has the strongest predicted intensity of any of the Fe IX lines between 175 and 180 Å, which is why it is also an excellent candidate for matching feature 6, discussed below, which is stronger than feature 5. Another possibility, thus, is that feature 5 is produced by an unknown Fe X line.

4.6. Feature 6

Like feature 5 and feature 7, feature 6 is likely produced by one or more Fe IX or Fe X lines. It has a wavelength of 176.80 ± 0.10 Å. As mentioned in the discussion of feature 5, the predicted intensity of the $3s^2 3p^5 3d\ ^3F_4$–$3s^2 3p^4 3d^2\ ^3D_3$ Fe IX transition at 177.418 Å makes it a good possibility for feature 6.

Young & Landi (2009) have identified the $3s^2 3p^5 3d\ ^3F_4$–$3s^2 3p^4 3d^2\ ^3D_3$ transition in *Hinode* spectra to be at 176.959 Å, which puts this line at the location of feature 6. We, thus, can confirm their identification. This line, however, is not yet listed in CHIANTI as a verified line.

4.7. Feature 7

Feature 7 at 178.80 ± 0.10 Å is 2 Å away from feature 6. Our measurements indicate that it is also formed by a low iron charge state. The second strongest theoretical Fe IX line in this region at 178.185 Å is the best candidate among the unverified lines in CHIANTI for this feature based on intensity. This line corresponds to the $3s^2 3p^5 3d\ ^3F_3$–$3s^2 3p^4 3d^2\ ^3D_2$ transition. But this line is too weak to represent the observed feature. Moreover, its position was assigned by Young & Landi (2009) to be located at 177.60 Å, which does not match the wavelength of feature 7.

Young & Landi (2009) have tentatively identified the position of the $3s^2 3p^5 3d\ ^3F_2$–$3s^2 3p^4 3d^2\ ^3D_1$ Fe IX transition at 178.71 or 178.99 Å (which compares to the wavelength of 179.26 Å listed in CHIANTI V7.0). Either wavelength would match that of feature 7. However, the predicted intensity is even lower than that of the $3s^2 3p^5 3d\ ^3F_3$–$3s^2 3p^4 3d^2\ ^3D_2$ transition (cf. Figure 6) so that we cannot confirm their identification.

4.8. Feature 8

Our measurements indicate that feature 8 is likely a composite of two (or more) lines. The first at 182.70 ± 0.05 Å is formed by a low iron charge state (Fe X or less). The second at 182.95 ± 0.08 Å is formed by a somewhat higher charge state (Fe XIII or less). There are no candidate lines in CHIANTI V7.0 that would match this feature.

Del Zanna (2012) finds an unidentified line at 182.916 Å in the *Hinode* EIS spectrum. Our measurements thus indicate that this is an iron line, probably from Fe XIII or less.

4.9. Feature 9

Feature 9 is seen at the lowest excitation energies only. Again, there are no candidate lines in CHIANTI that would match this feature. Its wavelength of 183.90 ± 0.08 is close to the two $2p$–$3s$ O VI lines at 183.94 and 184.12 Å, which may also have been observed by *SERTS* at 183.85 and 184.03 Å (Brosius et al. 1998).

The Livermore electron beam ion traps generally do not show any emission from low-Z ions such as oxygen, if the trap is filled with highly charged, heavy ions such as iron. The reason is that the heavier ions quickly displace the light ions (Marrs 2008). However, at low electron beam energies, the charge of the heavy ions is comparable to that the light ions, and the displacement effect is less efficient. As a result, we cannot rule it out completely that very small amounts of oxygen emission show up in our spectra at the low electron beam energies, which then disappears as the energy is raised. This would mimic the emission from a low ionization state of iron. But see our discussion of feature 18.

4.10. Feature 10

Feature 10 forms at higher electron energies than features 1–9 with the exception of feature 8b. Nevertheless, it appears that it is, at least in part, also an Fe IX line. The $3s^2 3p^5 3d\ ^1P_1$–$3s^2 3p^5 4p\ ^1S_0$ transition was recently identified by Young (2009) at 197.86 Å, and this line is now included in CHIANTI V7.0 (Landi et al. 2012). The position of the line and its predicted intensity (relative to the other Fe IX lines we have associated with various features above) are an excellent match for feature 10, which is located at 197.98 ± 0.09 Å.

4.11. Feature 11

Feature 11 at 199.40 ± 0.15 Å only forms at the higher electron energies. This indicates that it is from Fe XIII or a higher charge state. Del Zanna (2012) lists three unidentified features in the solar spectrum from *Hinode* that match the measured wavelength of feature 11. These are at 199.239, 199.338, and 199.598 Å. Unlike earlier versions of CHIANTI, CHIANTI V7.0 lists an Fe XIII line at 199.233 Å associated with the transition $3s 3p^3\ ^3D_3$–$3s^3 p^2 3d\ ^3F_4$. This transition matches feature 11 very well, and our measurement thus confirms the identity of this feature.

4.12. Feature 12

Feature 12 at 212.60 ± 0.10 Å is associated with the presence of Fe XII in our trap. The wavelength is too long to be seen with *Hinode*, and there are no candidate lines in CHIANTI.

4.13. Feature 13

Like feature 12, feature 13 at 215.90 ± 0.10 Å cannot be observed with *Hinode*, and there are no candidate lines in CHIANTI. The line seems to be associated with charge states Fe XIII or higher.

4.14. Feature 14

Feature 14 at 220.90 ± 0.10 Å forms already at lower electron beam energies and it is associated with charge states Fe XI or lower. CHIANTI V7.0 list a theoretical Fe XI line at 221.082 Å. This line is predicted to be the strongest Fe XIV line in this region with twice the strength of the Fe XI line at 223.6 Å. This makes it an excellent candidate for this feature. Hence, we tentatively identify feature 14 as the $3s^2 3p^4\ ^3P_2$–$3s^2 3p^3 3d\ ^3G_3$ transition in Fe XI.

4.15. Feature 15

Feature 15 at 225.25 ± 0.12 Å forms at even lower electron beam energies than feature 14. CHIANTI V7.0 list an unverified Fe VIII line at 225.291 Å. It has a predicted intensity of about half of the close-by Fe VIII line at 224.3 Å, and it, therefore, should be observed in our spectrum. As a result, this line is an excellent candidate for forming feature 15, and we identify feature 15 as the $3p^6 3d\ ^2D_{5/2}$–$3p^5 3d^2\ ^2P_{3/2}$ transition in Fe VIII.

4.16. Feature 16

Like feature 15, feature 16 at 226.35 ± 0.10 Å forms at low electron beam energies, and it is likely produced by an iron charge state Fe X or lower. In addition to the unverified Fe VIII line assigned to feature 15 above, CHIANTI lists a second unverified Fe VIII line in this region. It has a predicted wavelength of 227.096 Å and a predicted intensity of about a

quarter of the intensity of the close-by, known Fe VIII line at 224.3 Å. Therefore, it should also be observed in our spectrum, making it an excellent candidate for forming feature 16. We, thus, identify feature 16 as the $3p^6 3d\ ^2D_{3/2}$–$3p^5 3d^2\ ^2P_{1/2}$ transition in Fe VIII.

4.17. Feature 17

Feature 17 at 230.06 ± 0.08 Å is associated with the presence of Fe XIII in our trap. Therefore, we can rule out the Fe XXII line listed in CHIANTI close to this wavelength, as it cannot be produced at the energies of our measurement. CHIANTI V7.0 also lists a theoretical Fe X line 0.6 Å away at 230.667 Å. We can rule out this line as well because its ionization state is much lower than the approximate state we determined experimentally Feature 17, thus, remains unidentified.

4.18. Feature 18

Like feature 17, feature 18 at 233.50 ± 0.10 Å is associated with the presence of Fe XIII in our trap. It is close to an Fe XIII line, which in CHIANTI V7.0 is given a wavelength at 233.22 Å. This line would need to be more intense and shift in wavelength to match the observed feature 18.

Feature 18 matches in wavelength the location of the O IV $2p$–$3d$ transitions. As we already have pointed out in our discussion of feature 9, it is unlikely that there is sufficient oxygen in the trap to produce this feature. It is even more unlikely that oxygen produces this feature, because feature 18 correlates with the presence of Fe XIII in the trap. By contrast, feature 9 was correlated with lower charge states of iron, although the charge state of oxygen require to produce feature 9 would be higher. This contradiction makes it very unlikely that features 9 and 18 are formed by oxygen ions.

4.19. Feature 19

Like features 17, 18, and 20, feature 19 at 234.60 ± 0.10 Å is associated with the presence of Fe XIII in our trap (cf. Table 1). There are no candidate Fe XIII lines in CHIANTI near this wavelength.

4.20. Feature 20

Like the previous features, feature 20a at 238.50 ± 0.08 Å is also associated with the presence of Fe XIII in our trap. There are no unverified Fe XIII lines in CHIANTI with sufficient intensity near this wavelength.

Feature 20a also matches in wavelength the location of the O IV $2p$–$3d$ transitions. The peak, however, disappears at lower beam energies, when Fe XIII is no longer produced (cf. discussion of feature 18).

We find that this feature shifts to a wavelength of 238.20 ± 0.10 Å at lower beam energies. This indicates that it is possibly a blend with a line from Fe X or lower. CHIANTI V7.0 lists a verified candidate line from Fe VIII at 238.328 Å. The associated transition, $3p^6 3d\ ^2D_{5/2}$–$3p^6 4s\ ^2S_{1/2}$, is an electric quadrupole transition. The intensity of the line is rather weak (cf. Figure 4) and it does not account for the intensity of feature 20b.

5. LINE IDENTIFICATION IN THE 200–205 Å REGION

The identification of the iron $n = 3$ to $n = 3$ transitions in the 5 Å wide region between 200 and 205 Å has been controversial. In a detailed discussion of the spectral intensities in this region, Yamamoto et al. (2008) have previously shown that some of the wavelengths provided by the NIST Atomic Spectra Database V3.0 (NIST 2012) for Fe XIII are likely in error. One Fe XIII line in particular differed by 0.7 Å in the NIST database from CHIANTI. Lines in other iron charge states may also be associated with the wrong wavelength, as spectral fits by Yamamoto et al. (2008) using wavelengths from the CHIANTI model produced better fits of the experimental data than using wavelengths from NIST. The newest release of the NIST Atomic Spectra Database V4.0 continues to list the same wavelengths as V3.0.

The disagreement in the wavelengths in the CHIANTI model and the NIST database appears to be localized to the 200–205 Å region. A summary of the wavelengths of the Fe XI, Fe XII, and Fe XIII wavelengths, as given by CHIANTI V5.1 (used by Yamamoto et al. (2008)), CHIANTI V7.0, and NIST, is presented in Table 2. In order to investigate possible misidentifications of iron lines in either the CHIANTI or the NIST databases, we have made a detailed study of the lines observed in the 200–205 Å region.

A close-up view of the iron emission near 200 Å is given in Figure 7. The strongest lines in this region are from Fe XI at 188 Å, from Fe XII at 195 Å, and from Fe XIII at 204 Å. These three charge states of iron also produce all the weaker lines seen in this wavelength region. Thus, the three strongest lines represent markers of the abundance of the iron charge states in the EBIT-II plasma, when the electron beam energy is varied.

The middle panel of Figure 7 shows the spectra measured on EBIT-II at three different electron beam energies. These energies provide increasing amounts of line emission from Fe XIII: none in the red spectral trace, little in the blue spectral trace, and an amount on par with that from Fe XI and Fe XII in the green trace. Using the spectral changes as more higher charge states of iron are produced as a guide, we have identified the parentage of the lines that were in dispute in the analysis of Yamamoto et al. (2008) and for which the wavelengths in the CHIANTI model differ from the NIST database.

Our line identifications are shown in Figure 7(b). For comparison, we show the spectral model based on the CHIANTI wavelengths in Figure 7(a) and that based on the NIST critically evaluated wavelengths, as provided by Shirai et al. (2000), in Figure 7(c). There are no differences in the assigned wavelengths for lines below 200 Å. We show this wavelength region, however, to illustrate the changes in the experimental spectra, as the electron beam energy varies. For example, the feature labeled B, which is associated with an Fe XIII line, only appears in the green spectral trace, while line C, which is associated with an Fe XI line, is visible in all three spectra.

Our measurements confirm the identifications and wavelengths provided in CHIANTI. For example, the intensity variation of the feature we label *NOP* in Figure 7(b), which is very similar to that of the feature labeled A, indicates a blend with an Fe XII line. This is in agreement with the CHIANTI predictions. The NIST database, however, claims that the Fe XII line *N* is situated on the short-wavelength side of this feature, which would leave the feature at 204 Å comprised of two Fe XIII lines. We find no evidence for the existence of an Fe XII line at that location. We find instead a weak line at this location, which is commensurate with the Fe XIII line *M*. Similarly, we cannot find an Fe XII line at the NIST location for line *I*. This line probably blends with another Fe XII line, and we adopt the CHIANTI prediction that it is co-located with the Fe XII line *H*. Moreover, we find that the Fe XIII line *K* shows up only in spectra with a strong presence of Fe XIII. It is, therefore, not blended with the Fe XII

Table 2
Comparison of Wavelengths (in Å) Listed by CHIANTI and by NIST

Key	Transition	$\lambda_{\text{CHIANTI V5.1}}$	$\lambda_{\text{CHIANTI V7.0}}$	λ_{NIST}	Comment
		Fe XI			
	$^3P_2$–$^3D_3$	...	201.113	...	
G_{old}, L_{new}	$^3P_2$–$^3P_2$	201.577	**202.424**	**201.575**	
G_{new}	$^1D_2$–$^3S_1$	...	201.735	...	
L	$^1D_2$–$^1P_1$	**202.706**	**202.706**	**201.737**	
		Fe XII			
F	$^2P_{3/2}$–$^2P_{3/2}$	201.140	201.140	201.121	
H	$^2P_{1/2}$–$^2P_{1/2}$	**201.740**	**201.740**	**202.090**	
I	$^2P_{3/2}$–$^2S_{1/2}$	**201.760**	**201.760**	**200.356**	
J	$^2D_{3/2}$–$^2D_{5/2}$	**201.864**	**201.864**	**201.493**	Too weak to observe
N	$^2D_{5/2}$–$^2D_{5/2}$	**203.728**	**203.728**	**203.272**	
R	$^2P_{3/2}$–$^2P_{1/2}$	**204.382**	**204.382**	**204.743**	Too weak to observe
		Fe XIII			
D	$^3P_1$–$^3D_2$	200.022	200.022	200.021	
E	$^3P_1$–$^3D_1$	201.128	201.126	201.121	
K	$^3P_0$–$^3P_1$	202.044	202.044	202.044	
M	$^3P_1$–$^3P_0$	**203.164**	**203.165**	**202.424**	
O	$^3D_1$–$^3F_2$	...	203.722	...	
O	$^3P_2$–$^3D_2$	203.797	203.796	203.793	
P	$^3P_2$–$^3D_3$	203.828	203.827	203.826	
Q	$^3P_1$–$^1D_2$	204.263	204.263	204.263	
S	$^3P_2$–$^3D_1$	204.942	204.942	204.942	

Notes. The key corresponds to the labels used in Figure 7. The wavelengths of lines in disagreement are in boldface.

line *H*, in contradiction to the location assigned by the NIST database to line *H*. We find that line *H* contributes to the feature on the short-wavelength side of line *K* (together with *I*) which at lower electron beam energies is formed by line *G* in Fe XI. We note that in CHIANTI V5.1 *G* is formed by the $^3P_2$–$^3P_2$ transition at 201.577 Å, while in CHIANTI V7.0 it is formed by the $^1D_2$–$^3S_1$ transition at 201.735 Å. The latter provides a better fit.

According to the NIST database, line *G* would blend with line *L*, which is another Fe XI line, and with no line from a higher charge state. This contradicts the intensity pattern observed in our measurements. As mentioned above, line *G* is blended instead with Fe XII lines. The NIST wavelength of line *L* is, thus, doubtful as well. In agreement with the CHIANTI wavelength, we find a weak line at the NIST location of line *M*, i.e., lines *L* at 202.706 Å and L_{new} at 202.424 Å. This behaves like an Fe XI line and not like an Fe XIII line. Thus, we again confirm the CHIANTI predictions. This means that the Fe XIII line *M* in the NIST database must have a different wavelength, and, as we already mentioned above, this line assumes the NIST wavelength of the Fe XII line *N*, and line *N* blends with the Fe XIII lines *O* and *P*.

An overview of the NIST wavelengths that are in need of revision is listed in boldface in Table 2. The wavelengths of the Fe XI lines *L* and *M* shift by a full Å.

Out of six Fe XII lines in this wavelength interval, our experiments confirm that three are in a different location than given by NIST. These are lines *H*, *I*, and *N*, which shift by −0.3, +1.4, and +0.5 Å. Two other lines have been assigned a different wavelength in CHIANTI than by NIST. These lines shift by ±0.4 Å. They are, however, too weak to positively identify in our experimental spectra, and we cannot confirm the need for a revised line assignment.

Among the eight Fe XIII lines in the interval of interest, we find that only one NIST wavelength needs revision, i.e., line *M*. The shift is about 0.7 Å.

6. DISCUSSION AND SUMMARY

Our laboratory measurements of the 3–3 emission from Fe VIII through Fe XVI in the range 170–290 Å have found excellent agreement with predictions from the CHIANTI spectral model and database. This agreement extends to line assignments, line intensities, and line positions.

A total of 20 weak features were noted in the laboratory data that were absent in CHIANTI V5.1 and 18 that are currently absent in CHIANT V7.0. In addition to determining the wavelength of a given feature, we have noted the ionization state associated with each feature. Our analysis of features 10 and 11 agrees with lines added to CHIANTI V7.0, and thus confirm the additions.

The theoretical lines listed in CHIANTI V7.0 for Fe IX have been of limited value and could not be used to identify the feature we measured. The reason is that the number of theoretical Fe IX lines is too large and the predicted wavelength uncertainty too high to make reasonable assignments. An exception is feature 6, which we could identify based on the theoretical intensity given in CHIANTI and the wavelength measured by Young & Landi (2009). By contrast, the unverified lines listed in CHIANTI V7.0 for Fe VIII, the energies of which were taken from calculations by Griffin et al. (2000), allowed us to make tentative assignments of features 15 and 16. In particular, we associated features 15 and 16 with the $3p^6 3d\ ^2D_{5/2}$–$3p^5 3d^2\ ^2P_{3/2}$ and the $3p^6 3d\ ^2D_{3/2}$–$3p^5 3d^2\ ^2P_{1/2}$ transitions in Fe VIII at 225.25 ± 0.12 and 226.35 ± 0.10 Å, respectively. We also have tentatively assigned feature 14 at 220.90 ± 0.10 Å to the $3s^2 3p^4\ ^3P_2$–$3s^2 3p^3 3d\ ^3G_3$ transition in Fe XI based on the unverified lines in CHIANTI taken from Del Zanna (2010).

Most other features remain unidentified.

Five lines in Fe XI, Fe XII, and Fe XIII between 200 and 205 Å were noted for which NIST wavelengths do not agree with our observations, while the wavelengths provided by CHIANTI are

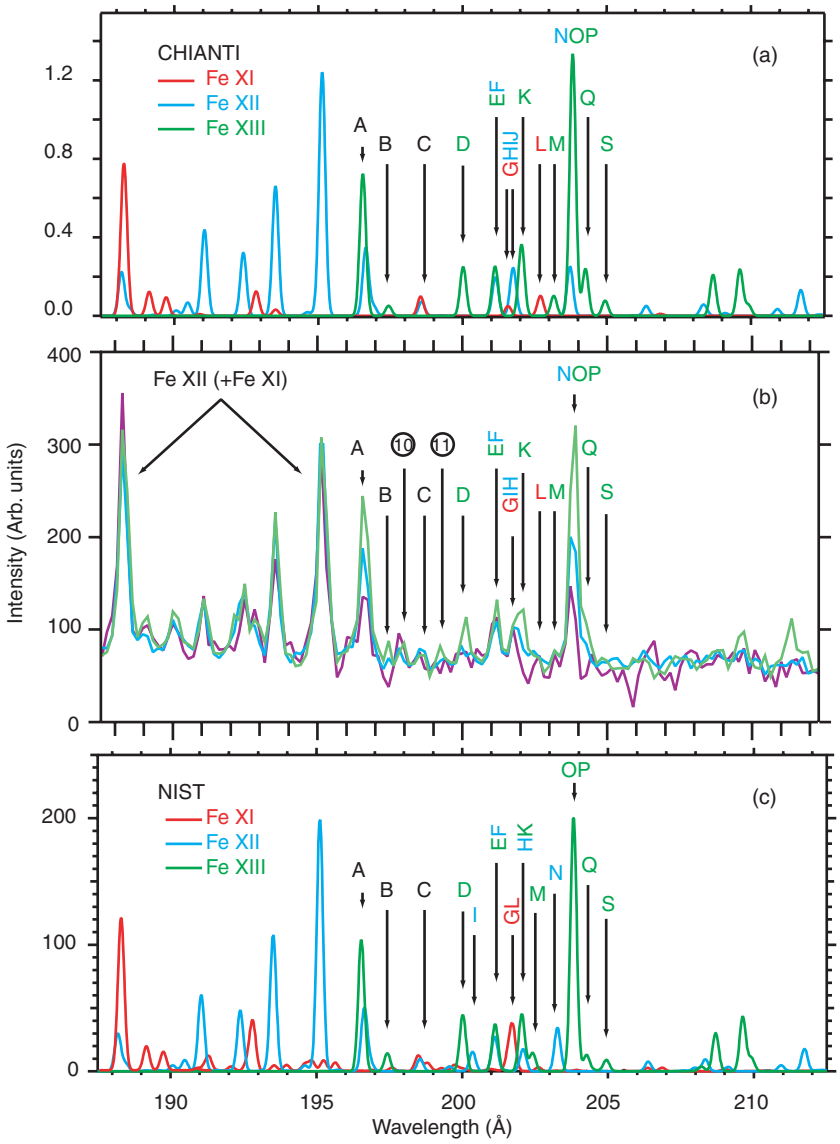

Figure 7. Detailed iron emission between 188 and 212 Å. (a) Predictions from the CHIANTI model; (b) spectrum recorded on the EBIT-II electron beam ion trap at Livermore at different electron beam energies to vary the amount of Fe^{10+}, Fe^{11+}, and Fe^{12+} ions in the trap; (c) predictions using NIST wavelengths and excitation data from Aggarwal & Keenan (2004). Features that are not reproduced by any of the models are labeled 10 and 11. The labels of features *D* through *S* match those listed in Table 2.

(A color version of this figure is available in the online journal.)

in good agreement with our measurements. The discrepancy between the NIST and CHIANTI wavelengths is not a simple change of position. The discrepancy means in effect that the line assignments in the NIST database need to be revised, i.e., lines that were thought to be from one charge state of iron are, indeed, from another charge state of iron.

The NIST wavelengths in this interval seem to trace to solar and laboratory identifications of Bromage et al. (1977, 1978). Their line assignments were evaluated by Shirai et al. (2000) at NIST and included in the NIST online database. The identifications made by Bromage et al. (1977, 1978), however, appear to be purely based on theoretical calculations, and no spectra have been presented in their papers. By contrast, the wavelengths in CHIANTI that do not agree with the NIST values come from identifications from Jupen et al. (1993) and Penn & Kuhn (1994) for Fe XIII, from Del Zanna & Mason (2005) for Fe XII, and from Jupen et al. (1993) for Fe XI. In our analysis, we confirm the identifications made by these authors.

The line at 202.424 Å identified by Bromage et al. (1978) as an Fe XIII transition is according to our analysis an Fe XI transition instead. Similarly, the line at 202.090 Å, which they identified as an Fe XII transition, has to be an Fe XIII line instead. The same is true for the line at 203.272 Å, identified by Bromage et al. (1978) as an Fe XII transition. It is an Fe XIII transition by our analysis.

The Fe XII line located at 200.356 Å according to Bromage et al. (1978) does not exist in our analysis. However, Del Zanna (2012) has noted an unidentified feature at this position in *Hinode* EIS observations of the Sun. He also notes two other features in the EIS observations, which are at the wavelengths of the Bromage et al. (1978) 201.493 and 204.743 Å lines. Del Zanna (2012) assigns iron charge states lower than Fe XII, in disagreement with Bromage et al. (1978) and NIST. Since these

lines are too weak for us to observe, we cannot confirm these different assignments.

The misidentification by Bromage et al., unfortunately, continues to be perpetuated in the NIST data base. Until the NIST database has been updated, it appears that CHIANTI provides better spectroscopic data for iron than NIST.

This work was supported by NASA's Solar and Heliospheric Physics Program under grant No. NNX07AH98G. Work at the Lawrence Livermore National Laboratory was performed under the auspices of the Department of Energy under contract No. DE-AC52-07NA-27344.

REFERENCES

Aggarwal, K. M., & Keenan, F. P. 2004, A&A, 418, 371
Beiersdorfer, P. 2003, ARA&A, 41, 343
Beiersdorfer, P. 2008, Can. J. Phys., 86, 1
Beiersdorfer, P., Crespo López-Urrutia, J. R., Springer, P., Utter, S. B., & Wong, K. L. 1999a, Rev. Sci. Instrum., 70, 276
Beiersdorfer, P., Lepson, J. K., Brown, G., et al. 1999b, ApJ, 519, L185
Bromage, G. E., Cowan, R. D., & Fawcett, B. C. 1977, Phys. Scr., 15, 177
Bromage, G. E., Cowan, R. D., & Fawcett, B. C. 1978, MNRAS, 183, 19
Brosius, J. W., Davila, J. M., & Thomas, R. J. 1998, ApJS, 119, 255
Brown, G. V., Beiersdorfer, P., Chen, H., Chen, M. H., & Reed, K. J. 2001, ApJ, 557, L75
Chen, H., Beiersdorfer, P., Heeter, L. A., et al. 2004, ApJ, 611, 598
Chen, H., Beiersdorfer, P., Scofield, J. H., et al. 2002, ApJ, 567, L169
Del Zanna, G. 2009, A&A, 508, 501
Del Zanna, G. 2010, A&A, 514, A41
Del Zanna, G. 2011, A&A, 533, A12
Del Zanna, G. 2012, A&A, 537, A38
Del Zanna, G., & Mason, H. E. 2005, A&A, 433, 731
Del Zanna, G., Storey, P. J., & Mason, H. E. 2010, A&A, 514, A40
Dere, K. P., Landi, E., Mason, H. E., Fossi, B. C. M., & Young, P. R. 1997, ApJS, 125, 149
Dere, K. P., Landi, E., Young, P. R., et al. 2009, A&A, 498, 915
Drake, J. J., Swartz, D. A., Beiersdorfer, P., Brown, G. V., & Kahn, S. M. 1999, ApJ, 521, 839
Griffin, D., Pindzola, M., & Badnell, N. R. 2000, A&ASS, 142, 217
Gu, M., Kahn, S., Savin, D., et al. 1999, ApJ, 518, 1002
Ishikawa, Y., & Vilkas, M. J. 2008, Phys. Rev. A, 78, 042501
Jupen, C., Isler, R. C., & Träbert, E. 1993, MNRAS, 264, 627
Landi, E., Del Zanna, G., Young, P. R., Dere, K. P., & Mason, H. E. 2012, ApJ, 744, 99
Landi, E., Del Zanna, G., Young, P. R., et al. 2006, ApJS, 162, 261
Lemen, J. R., Title, A. M., Akin, D. J., et al. 2012, Sol. Phys., 275, 17
Lepson, J. K., Beiersdorfer, P., Brown, G. V., et al. 2000, RevMexAA, 9, 137
Lepson, J. K., Beiersdorfer, P., Brown, G. V., et al. 2002, ApJ, 578, 648
Lepson, J., Beiersdorfer, P., Hurwitz, M., et al. 2008, J. Phys. Conf. Ser., 130, 012014
Liang, G. Y., Badnell, N. R., Crespo López-Urrutia, J. R., et al. 2010, ApJS, 190, 322
Liang, G. Y., Baumann, T. M., Crespo L opez-Urrutia, J. R., et al. 2009, ApJ, 696, 2275
Marrs, R. E. 2008, Can. J. Phys., 86, 11
NIST 2012, NIST Standard Reference Database, Version 4, http://www.nist.gov/pml/data/asd.cfm
O'Dwyer, B., Badnell, G. D. N. R., Mason, H. E., & Storey, P. J. 2012, A&A, 537, A22
Penn, M. J., & Kuhn, J. R. 1994, ApJ, 434, 807
Savin, D. W., Beiersdorfer, P., Crespo López-Urrutia, J., Decaux, V., & Gullikson, E. M. 1996, ApJ, 470, L73
Schmitt, J. H. M. M., Drake, J. J., Haisch, B. M., & Stern, R. A. 1996a, ApJ, 467, 841
Schmitt, J. H. M. M., Drake, J. J., Stern, R. A., & Haisch, B. M. 1996b, ApJ, 457, 882
Schrijver, C. J., Mewe, R., van den Oord, G. H. J., & Kaastra, J. S. 1995, A&A, 302, 438
Shirai, T., Sugar, J., Musgrove, A., & Wiese, W. L. 2000, J. Phys. Ref. Data, Monograph 8 (Melville, NY: AIP)
Sirk, M. M., Hurwitz, M., & Marchant, W. 2010, Sol. Phys., 264, 287
Thomas, R. J., & Neupert, W. M. 1994, ApJS, 91, S461
Woods, T. N., Hock, R., Eparvier, F., et al. 2011, ApJ, 739, 59
Yamamoto, N., Kato, T., Funaba, H., et al. 2008, ApJ, 689, 646
Young, P. R. 2009, ApJ, 691, L77
Young, P. R., Del Zanna, G., Mason, H. E., et al. 2007, PASJ, 59, 857
Young, P. R., & Landi, E. 2009, ApJ, 707, 173
Zhitnik, I. A., Kuzin, S. V., Urnov, A. M., Keenan, F. P., & Pinfield, D. J. 1999, MNRAS, 308, 228